Check for updates

Photo-assisted electrochemical CO$_2$ reduction at a boron-doped diamond cathode†

Goki Iwai, [iD] Andrea Fiorani, [iD] * Jinglun Du [iD] and Yasuaki Einaga [iD] *

We report on the coupling of photoelectrochemical water oxidation and electrochemical CO$_2$ reduction to formic acid for a photoelectrochemical system capable of light and electrochemical energy conversion to chemical energy. Titanium oxide nanotubes (TiO$_2$ NT) and boron-doped diamond (BDD) electrodes were used as a photoanode and a cathode, respectively. From CO$_2$ electrochemical reduction at BDD, formic acid was obtained with a faradaic efficiency of about 86% and the system provided an overall energy conversion efficiency of 5.5%. From previous CO$_2$ reduction at a dark electrolyzer based on a BDD cathode, the cell voltage was reduced from 2.7 V to 1.4 V with 52% saving of the electrical energy input. This resulted in an increase from 50% to nearly 80% of electrical-to-chemical energy conversion efficiency.

Introduction

The utilization of carbon-based materials (*e.g.*, lignite, carbon monoxide, etc.) for the production of hydrocarbons has long been established, namely in 1913 with the Bergius process,[1] and in 1925 with the Fischer–Tropsch process.[2]

The evolution of these processes is nowadays pursued by the utilization of CO$_2$ as an alternative carbon feedstock,[3,4] therefore transformation into high-added value chemicals can be a favourable pathway for this C1-synthon utilization in chemical/organic synthesis.[5–9]

If the synthesis is conducted using electrochemical methods, the products of CO$_2$ reduction (*e.g.*, CO, formic acid, methane, C$_{2+}$ hydrocarbons, and oxygenates) might find application in the production of fine chemicals,[10,11] and in addition as carriers or storage materials for renewable electrical energy. Furthermore, CO$_2$ electrochemical reduction can be performed under ambient conditions, even at the industrial-scale.[3,12,13] In this case, to be competitive, this reaction must retain most of the energy in the final chemical product *i.e.*, high energy conversion efficiency, or low activation energy for CO$_2$,[14] and electrochemical (EC) and photoelectrochemical (PEC) approaches have been investigated for CO$_2$ reduction.[15] This may help produce energy with a lower environmental impact,[16–18] as in the case of hydrogen production from water electrolysis.[19–22]

In a (photo)electrochemical system, energy efficiency is affected by several energy losses, mainly ascribed to the

electrochemical cell (*e.g.*, ohmic drop, electrolyte, mass transport, and separators),[23,24] which can be reduced by a careful engineering design, and the overpotential that is intrinsic for the reaction and electrocatalyst/electrode materials used. In particular, when a reduction reaction is coupled with the oxygen evolution reaction (OER) from water oxidation, this 4-electron reaction may account for the largest loss of energy in the electrochemical system due to overpotential.[25]

This problem has been tackled by the use of several metal oxides as highly active electrocatalysts for the OER.[26,27]

In this context, we demonstrated previously that in a CO$_2$ electrolyser the right choice of the anode material improved the electric-to-chemical energy conversion efficiency up to 50%.[28]

To further decrease the reliance on electrical energy, we present here a photoelectrochemical system comprising titanium oxide nanotubes (TiO$_2$ NTs) and boron-doped diamond (BDD) electrodes as a photoanode and a cathode, respectively. A BDD electrode has been selected for its high faradaic efficiency for formic acid (FA) production from CO$_2$ reduction, and in fact it can prevent the side reaction of proton reduction which competes with CO$_2$ reduction by its wide potential window and high overpotential for hydrogen evolution,[28–30] and long term stability.[31,32] TiO$_2$ NTs were selected as a photoanode because they can drive water oxidation at negative potentials under light illumination compared to conventional metal oxide electrodes,[33] and in addition, nanotubes can expose a larger surface area than flat electrodes.[34,35]

The objective was to develop a PEC system with the ability of photo-assisted water oxidation at the TiO$_2$ NT electrode coupled with electrochemical CO$_2$ reduction to formic acid, and evaluate its energy efficiency as the main figure of merit. Finally, the energy efficiency of the present PEC system was compared with that of a full EC system that we developed previously[28,29] to

Department of Chemistry, Keio University, Yokohama 223-8522, Japan.
E-mail: andrea.fiorani@keio.jp, einaga@chem.keio.ac.jp

evaluate the benefits of using photo-assisted electrochemical water oxidation and the viability of BDD as a cathode for CO_2 electrochemical reduction.

Experimental

Materials

Potassium chloride (KCl), potassium hydroxide (KOH), sulphuric acid (H_2SO_4), acetone (C_3H_6O), and isopropanol (C_3H_8O) were purchased from Wako Pure Chemical Industries Ltd. Ammonium dihydrogen phosphate [$(NH_4)H_2PO_4$] and ammonium fluoride–hydrofluoric acid ($NH_4F \cdot HF$) were purchased from Sigma-Aldrich. Formic acid for HPLC calibration was obtained from FUJIFILM Wako Pure Chemical Corporation, while hydrogen and carbon monoxide for GC calibration were obtained from GL Sciences. Carbon dioxide (purity over 99.990 vol%) was purchased from Resonac Gas Products Corporation, and nitrogen gas (purity over 99.99995 vol%) was purchased from Taiyo Nippon Sanso Corporation. All reagents were used as received. Titanium (thickness 0.2 mm) and platinum (thickness 1 mm, Φ 50 mm) plates were purchased from Nilaco Corp. (Japan). Ultrapure water was from a Simply-Lab water system (DIRECT-Q 3 UV, Millipore) with a resistivity of 18.2 MΩ·cm at 25 °C. Experiments were performed at room temperature (23–25 °C) and atmospheric pressure.

BDD fabrication and characterization: cathode

The polycrystalline BDD film was deposited on a Si (100) wafer substrate with a microwave plasma-assisted chemical vapor deposition (MPCVD) system (AX6500, Cornes Technologies Ltd.). The concentration of boron in the BDD film was set to be 0.1% according to the ratio between the carbon source (methane) and the boron source (trimethylborane).[28] The surface morphology of the BDD film was imaged with a scanning electron microscope (JCM-6000, JEOL) (Fig. S1, ESI†). The Raman spectrum was recorded using an Acton SP2500 (Princeton Instruments) with a 532 nm laser to confirm the diamond nature, boron inclusion and exclude the presence of sp^2 carbon (Fig. S1, ESI†).[28,29]

TiO$_2$ NT fabrication and characterization: photoanode

Titanium oxide nanotubes (TiO_2 NTs) were prepared by titanium foil oxidation in a fluorine electrolyte, a procedure adapted from previous reports.[35,36] A titanium plate was sonicated in acetone, isopropanol and water 10 minutes each, and dried under a nitrogen stream. The electrolyte solution consisted of 1 M $(NH_4)H_2PO_4$ and 0.5 wt% $NH_4F \cdot HF$ in ultrapure water. Using a DC power supply, a constant voltage of 30 V was applied between the Ti plate and Pt plate for 3 hours, followed by rinsing with ultrapure water. The TiO_2 NT plate was annealed at 450 °C for 1 hour (Program electric Furnace SMF-1, AS ONE Co.). The crystalline phase was investigated using an X-ray diffractometer (D8 ADVANCE, Bruker) with Cu-Kα radiation, and the surface was imaged with a field emission scanning electron microscope (FE-SEM-H2 SU70, Hitachi High-Tech Co.). The band gap was measured from the reflectance spectra obtained using a UV-3600

Plus UV-Vis-NIR spectrophotometer (Shimadzu). Details of the optimisation procedure to obtain TiO_2 NTs and characterization are available in the supporting information (Fig. S2, ESI†).

Electrochemistry

Electrochemical measurements were performed with a potentiostat/galvanostat system PGSTAT204 (Metrohm Autolab). Ag/AgCl, KCl sat'd was the reference electrode in all electrochemical measurements, and all potentials are referred to this electrode, except otherwise stated. Before each experiment, the BDD electrode was sonicated in isopropanol and ultrapure water for 10 min each. We proved that electrochemical pretreatment ensured surface cleanliness and the optimal electrochemical response of the BDD,[28,29] therefore several cyclic voltammetry (CV) scans (10 cycles from −3.5 V to 3.5 V, and 20 cycles from 0 V to 3.5 V in 0.1 M H_2SO_4 with a scan rate of 0.5 V s^{-1}) were performed before CO_2 reduction. Electrochemical measurements were conducted in a two-chamber polytetrafluoroethylene (PTFE) flow cell, both equipped with a reference electrode and separated by a Nafion NRE-212 (Sigma-Aldrich). BDD (0.1% B/C) and TiO_2 NTs were set as working and counter electrodes, with geometrical areas of 9.62 cm^{-2} and 12.56 cm^{-2}, respectively (Fig. S3, ESI†). This photoelectrochemical cell can be operated in a three-electrode configuration (a BDD working electrode, an Ag/AgCl, KCl sat'd reference electrode, and a TiO_2 NT counter electrode), and in a two-electrode configuration (a BDD cathode working electrode, and a TiO_2 NT photoanode counter electrode). The catholyte and anolyte were 0.5 M KCl (50 mL) and 0.5 M KOH (90 mL), respectively. Oxygen was removed from the catholyte by N_2 purging for 30 min and then CO_2 was bubbled for 60 min at 200 mL min^{-1}, resulting in a CO_2-sauturated solution. During electrolysis, CO_2 flow was set to be 30 mL min^{-1}. Each experiment has been repeated three times to confirm the results.

Product analysis

Quantification of the CO_2 reduction products was performed at the end of each experiment. Formic acid was quantified by high-performance liquid chromatography (HPLC, CDD-10A, Shimadzu Corp.). The gaseous products (CO and H_2) were collected in an aluminium gas bag (GL Sciences) and quantified by gas chromatography (GC-2014, Shimadzu Corp.). Calibration lines, LOD and Min–Max concentrations detected are available in Fig. S4 (ESI†).

Light source

Light irradiation was carried out using a SP11 Spot-cure (USHIO Inc., Japan). The lamp emission spectrum is available in Fig. S5 (ESI†). Light intensity was measured using a power meter (Solar power meter TM-207, MK Scientific, Inc.).

Energy conversion efficiency

To take into account the electric and light power injected into this photoelectrochemical system which provides a net conversion of sunlight in the form of a reduced electric bias, the energy

throughput conversion efficiency for photo-assisted electrolysis (η_{PAE}) can be calculated using eqn (1):[37,38]

$$\eta_{PAE} = \frac{P_{out}}{P_{in}} = \frac{E^0_{HCOOH/CO_2} \times i_{tot} \times FE_{HCOOH}}{E_{tot} \times i_{tot} + P_{light} \times A} \quad (1)$$

where P_{out} and P_{in} are the power (W), in and out from the system, respectively. E^0_{HCOOH/CO_2} is the standard potential for CO_2 reduction to formic acid (1.3997 V),[29] i_{tot} (A) is the total current flowing in the electrochemical cell, FE_{HCOOH} is the faradaic efficiency for formic acid production, E_{tot} (V) is the total voltage applied by the potentiostat between the cathode and photoanode electrodes, P_{light} (W cm^{-2}) is the power of light illumination, and A (cm^2) is the TiO_2 NT photoanode area.

The electrical-to-chemical energy (ECE) conversion efficiency (η_{ECE}) can be calculated using eqn (2).[29]

$$\eta_{ECE} = \frac{E^0_{HCOOH/CO_2} \times FE_{HCOOH}}{E_{tot}} \quad (2)$$

Results and discussion

The photoelectrochemical system capable of reducing CO_2 to formic acid developed here consists of a BDD cathode and a TiO_2 NT photoanode. We demonstrated the viability of electrochemical reduction of CO_2 on BDD achieving an optimised and stable process.[28,29] To further decrease the dependence on electrical energy for the whole electrochemical process of water oxidation (anode) and CO_2 reduction (cathode), we substituted the metal oxide anode with a TiO_2 NT photoanode. The TiO_2 NT electrode was fabricated by titanium oxidation and dissolution in a fluorine electrolyte, with optimization of parameters (Fig. S2, ESI†), such as electrolytic solution and oxidation time. The structure resulted in nanotubes of 200 nm in diameter (Fig. 1A) and the crystalline phase has been confirmed as anatase using

XRD (Fig. 1B, and SI 2.1, ESI†). The average band gap, measured using the diffuse reflectance spectra according to the Kubelka–Munk theory,[39] was 3.4 ± 0.1 eV (Fig. 1C and Fig. S2, ESI†), which is in agreement with the typical band gap energy of TiO_2 (anatase).[40] We should mention that band gaps down to 2 eV can be effectively obtained for TiO_2, and this has implication on the energy adsorption (e.g., from the solar radiation). This requires further processing of TiO_2 by doping with non-metals as carbon at high temperature,[34,35,41] or by metal doping as in SrTiO_3:Al.[42] However, this is beyond the scope of our present investigation. Finally, under our experimental conditions, the addition of HF compared to NH_4F only gave better results in terms of water oxidation current (Fig. 1D).

The flat band potential (E_{FB}) of TiO_2 NTs was evaluated by open circuit potential (OCP) measurements upon increasing the light intensity (Fig. S6, ESI†) because the OCP shifts towards the E_{FB} theoretically reaching it at sufficiently high illumination intensities.[43–45] The E_{FB} set at 0.1 V (vs. normal hydrogen electrode, NHE) at pH 0 with a Nernstian dependence as a function of pH (54 mV pH^{-1}, Fig. 2A) indicates that H$^+$ and
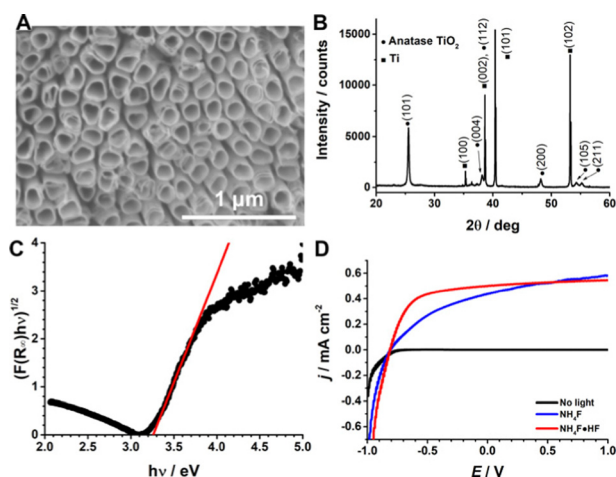
Fig. 1 Characterisation of TiO_2 NTs. (A) SEM micrograph, scale bar is 1 μm. (B) XRD spectrum. (C) Kubelka−Munk plot. (D) Photoelectrochemical response measured by cyclic voltammetry at 100 mV s^{-1} in 0.5 M KOH with light applied of 6.5 mW cm^{-2}, for TiO_2 NTs fabricated with addition of NH_4F (blue) or NH_4F·HF (red and black). Reference electrode: Ag/AgCl, KCl sat'd.
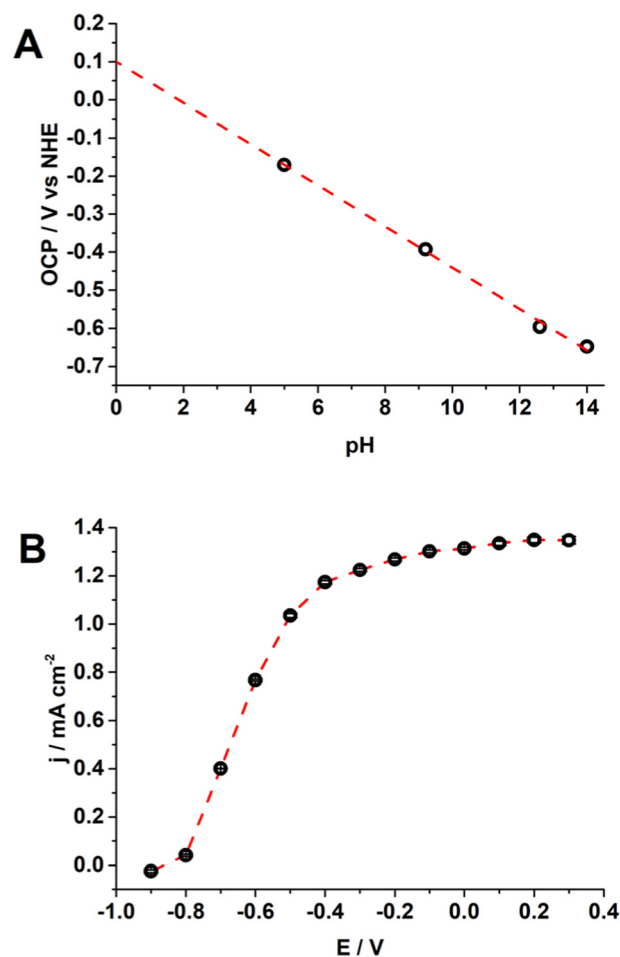
Fig. 2 (A) OCP under illumination in 0.1 M phosphate buffer, while pH 14 is 0.5 M KOH; reference electrode: NHE = Ag/AgCl, KCl sat'd + 0.197 V; standard error: 0.01 V. (B) Limiting current from chronoamperometry at selected potentials in KOH 0.5 M (light power: 25.2 mW cm^{-2}); reference electrode: Ag/AgCl, KCl (sat'd); the error bar shows the standard deviation (n = 3).

OH^- are potential determining ions (PDIs) adsorbed on the metal oxide surface within the Helmholtz layer.[46,47] The E_{FB} value is also in agreement with the potential for the onset of the photocurrent (Fig. 1D and 2B).[45,48] From this characterization, we assessed the fine quality of the TiO_2 NTs.

The electrochemical cell assembly for CO_2 reduction is depicted in Fig. 3 and Fig. S3 (ESI†). We used two configurations: (1) the potential at the BDD cathode was fixed compared to the Ag/AgCl, KCl (sat'd) reference electrode (*i.e.*, the potential at the TiO_2 NT electrode was floating, that is a three-electrode configuration), namely $E_{cathode}$; (2) the total voltage between the BDD cathode and the TiO_2 NT photoanode was fixed (*i.e.*, both TiO_2 NT and BDD potentials were floating, that is a two-electrode configuration), namely E_{tot}.

Configuration 1, that is a three-electrode configuration, of $E_{cathode}$ at -2.15 V *vs.* Ag/AgCl, KCl (sat'd) is meant to demonstrate that the faradaic efficiency for formic acid production can reach an adequate level (nearly 90%), as the potential at BDD ($E_{cathode}$) is in the optimal range, as we observed previously,[28,29] therefore the effectiveness of the photoelectrochemical cell can be assessed and the stability of the TiO_2 NT photoanode can be tested. η_{PAE} was measured at different light powers (from 6.5 to 35 mW cm^{-2}) and was compared with theoretical efficiency computed for 90% faradaic efficiency, combined with E_{tot} and current as in the range of values measured experimentally, from 1.4 V to 3 V and from 0.3 mA cm^{-2} to 0.7 mA cm^{-2}, respectively (Fig. S7 and S8, ESI†).

The potential at TiO_2 NTs is stabilised to around -0.55 V to -0.75 V *vs.* Ag/AgCl, KCl sat'd (Fig. S7B, ESI†), enough to provide the current measured at the BDD cathode (Fig. S7D and Fig. 2B, ESI†), and is therefore limited only by the kinetics

Fig. 3 Schematic diagram of the photoelectrochemical cell. The symbol ⊗ represents the reference electrode: Ag/AgCl, KCl (sat'd). $E_{cathode}$ means that the potential at the BDD cathode is fixed with respect to the reference electrode. E_{tot} means that the potential is fixed between the BDD and TiO_2 NT electrodes. The reference electrode in the TiO_2 NT electrode compartment is used to monitor the potential at TiO_2 NTs. Black lines are cable connections. In and Out are connecting tubes for electrolyte circulation. A quartz window permits the light to reach the TiO_2 NT photoanode.

of CO_2 reduction at BDD. The faradaic efficiency for formic acid production could reach an adequate value of 90% (range 79–94%, Table S1, ESI†) which confirmed the appropriate operation of the electrochemical cell in the cathodic reaction. A particular case is the irradiation with 6.5 mW cm^{-2} which is not sufficient to sustain water oxidation at a stable potential that gradually shifted positive, from -0.6 V to 2.6 V *vs.* Ag/AgCl, KCl sat'd (Fig. S7, ESI†).

When the photoelectrochemical cell is operated in configuration 2, that is a two-electrode configuration, we performed the CO_2 reduction at different E_{tot}, from 1 V to 2.4 V, and a light input of 25.2 mW cm^{-2} was selected from the highest efficiency obtained from configuration 1 (Fig. S8, ESI†). Moreover, this light power could maintain a stable potential at TiO_2 NTs during the CO_2 reduction (Fig. S7, ESI†).

The voltage range applied is 0.3 to 1.7 V lower than that of a conventional electrochemical cell without photo-assisted electrolysis (*i.e.*, E_{tot} = 2.7 V at the BDD cathode and Ir oxide anode).[28] Concerning this fundamental aspect, we have to recall that the cell does not convert directly light energy into chemical energy (*i.e.*, the photocurrent is zero without an external bias, Fig. S9, ESI†), however the overall effect is to lower E_{tot} and decrease the electrical power input.

In the range of E_{tot} investigated the current increased up to 1.7 mA cm^{-2}, and the faradaic efficiency for formic acid (the main product, together with a small amount of carbon monoxide and hydrogen, Table S2 and Fig. S10, S11 and S12) reached an average and stable value of 86% from 1.4 V onward (Fig. 4A).

At E_{tot} of 1.4 V, the potential measured at BDD was -2.04 V which is near the limit for CO_2 reduction to formic acid. In fact, for a lower potential at BDD (*i.e.*, < 2.0 V *vs.* Ag/AgCl, KCl sat'd, Fig. S10, ESI†), the kinetics for the formation of a CO_2 radical anion becomes slow, and this is the rate determining step on an inert electrode such as BDD where the CO_2 radical anion is loosely absorbed[30,32] with a consequent increase of proton reduction to hydrogen. On the other hand, E_{tot} higher than 1.4 V increased only the reduction rate of CO_2 (*i.e.*, the current increased along with the potential at BDD), while did not enhance the faradaic efficiency further.

It is possible to translate this combined effect of current and faradaic efficiency directly on the energy throughput conversion efficiency (Fig. 4B). η_{PAE} is limited by both faradaic efficiency and current below 1.4 V, while it is mainly limited by the current above 1.4 V. Therefore, the flattening of η_{PAE} at 5.5% was ascribed to the limited current available in this system and set by the TiO_2 NT electrode (Fig. 2 and Fig. S10, ESI†).

While η_{PAE} is the optimal descriptor for a PEC system, combining both light and electrical energies in the conversion to chemical energy, we would present all figures of merit for the system under investigation.

The electrical-to-chemical conversion efficiency accounts only for the electrical energy input, however it can be reported also for PEC systems (Table S3, ESI†).[49–51]

This permits a direct comparison with our previous electrochemical CO_2 reduction at BDD, furthermore evaluating explicitly the effect of the TiO_2 NTs on water oxidation.
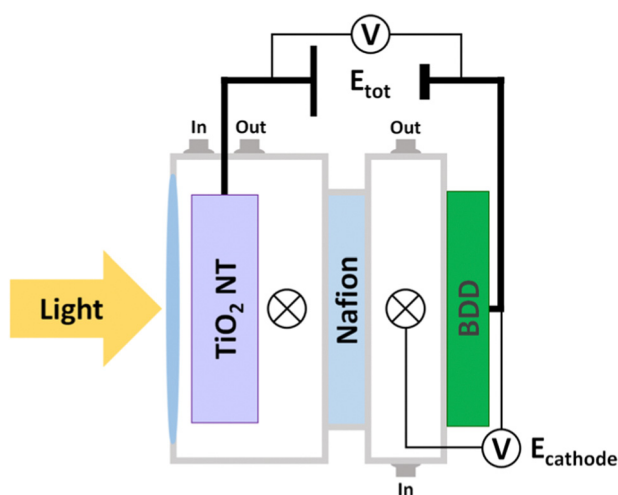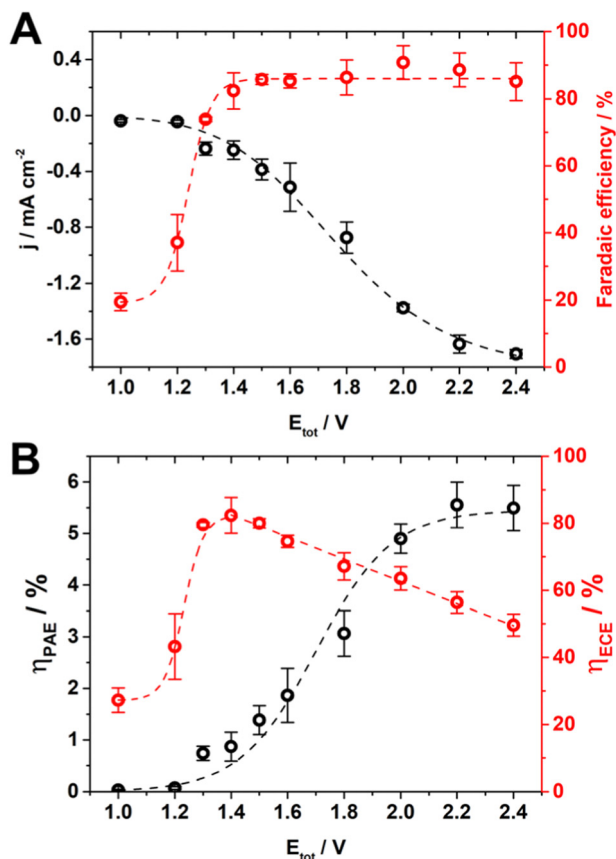
Fig. 4 (A) Average current measured at the BDD cathode (black) and faradaic efficiency for the production of formic acid (red). (B) Energy throughput conversion efficiency for photo-assisted electrolysis (η_{PAE}, black), and electric-to-chemical energy conversion efficiency (η_{ECE}, red) as a function of E_{tot} in configuration 2. Light intensity: 25.2 mW cm^{-2}. Lines are only a guide for the eye. The error bar shows the standard deviation ($n = 3$).

η_{ECE} reaches a stable 80% in the range 1.3–1.5 V (Fig. 4B) compared to 50% reached previously without photo-assisted electrolysis at 2.7 V,[28] which saved 52% of electrical energy. This energy saving is evident from the potential at TiO_2 NTs for water oxidation in the range of -0.75 to -0.67 V (Fig. S10, ESI†) compared to 0.5 V observed experimentally[28] (theoretical 0.21 V, see ESI† Section 15).

Conclusions

We developed an electrolyser to convert carbon dioxide to formic acid with faradaic efficiency reaching 86%. The system comprised a photoanode made of titanium oxide (anatase) nanotubes for photoelectrochemical water oxidation and a boron-doped diamond cathode for CO_2 electrochemical reduction to formic acid. This photoelectrochemical cell could convert light power, in the form of a reduced electric bias, to chemical with an efficiency of 5.5%, reaching 80% of electrical-to-chemical conversion efficiency. A further improvement in this photoelectrochemical system will be the coupling of a photovoltaic module with an electrolyser consisting of an oxide anode and a BDD cathode to

evaluate the solar to energy conversion efficiency and the viability of BDD as a profitable cathode for CO_2 electrochemical reduction. This approach is currently under investigation in our laboratory.

Author contributions

Goki Iwai: methodology, investigation, formal analysis, visualization, and writing – original draft. Andrea Fiorani: conceptualization, supervision, methodology, investigation, formal analysis, validation, and writing – original draft. Jinglun Du: methodology and validation. Yasuaki Einaga: conceptualization, supervision, and funding acquisition. All authors: writing – review and editing.

Conflicts of interest

There are no conflicts to declare.

Acknowledgements

References

1 Z. Wang, *Comprehensive Organic Name Reactions and Reagents*, John Wiley & Sons Ltd., Hoboken, USA, 2009, 397–340.
2 M. E. Dry, *Catal. Today*, 2002, **71**, 227–241.
3 R. I. Masel, Z. Liu, H. Yang, J. J. Kaczur, D. Carrillo, S. Ren, D. Salvatore and C. P. Berlinguette, *Nat. Nanotechnol.*, 2021, **16**, 118–128.
4 C. Chen, M. Garedew and S. W. Sheehan, *ACS Energy Lett.*, 2022, 7, 988–992.
5 M. Aresta, A. Dibenedetto and A. Angelini, *Chem. Rev.*, 2014, **114**, 1709–1742.
6 C. M. Rayner, *Org. Process Res. Dev.*, 2007, **11**, 121–132.
7 R. Matthessen, J. Fransaer, K. Binnemans and D. E. De Vos, *Beilstein J. Org. Chem.*, 2014, **10**, 2484–2500.
8 L. Lombardi, A. Cerveri, L. Ceccon, R. Pedrazzani, M. Monari, G. Bertuzzi and M. Bandini, *Chem. Commun.*, 2022, **58**, 4071–4074.
9 G. Fiorani, W. Guo and A. W. Kleij, *Green Chem.*, 2015, **17**, 1375–1389.
10 J. Seidler, A. Roth, L. Vieira and S. R. Waldvogel, *ACS Sustainable Chem. Eng.*, 2023, **11**, 390–398.
11 R. Matthessen, J. Fransaer, K. Binnemans and D. E. De Vos, *Beilstein J. Org. Chem.*, 2014, **10**, 2484–2500.
12 Y. Cheng, P. Hou, X. Wang and P. Kang, *Acc. Chem. Res.*, 2022, **55**, 231–240.
13 A. Löwe, M. Schmidt, F. Bienen, D. Kopljar, N. Wagner and E. Klemm, *ACS Sustainable Chem. Eng.*, 2021, **9**, 4213–4223.
14 S. Matsuda, M. Tanaka and M. Umeda, *Anal. Methods*, 2022, **14**, 3280–3288.
15 J. He and C. Janaky, *ACS Energy Lett.*, 2020, **5**, 1996–2014.

16 C. A. Martinez-Huitle, M. A. Rodrigo, I. Sires and O. Scialdone, *Appl. Catal., B*, 2023, **328**, 122430.

17 S. O. Ganiyu and C. A. Martinez-Huitle, *Curr. Opin. Electrochem.*, 2020, **22**, 211–220.

18 S. O. Ganiyu, C. A. Martinez-Huitle and M. A. Rodrigo, *Appl. Catal., B*, 2020, **270**, 118857.

19 J. C. Ehlers, A. A. Feidenhans'l, K. T. Therkildsen and G. O. Larrazábal, *ACS Energy Lett.*, 2023, **8**, 1502–1509.

20 M. Chatenet, B. G. Pollet, D. R. Dekel, F. Dionigi, J. Deseure, P. Millet, R. D. Braatz, M. Z. Bazant, M. Eikerling, I. Staffell, P. Balcombe, Y. Shao-Horn and H. Schäfer, *Chem. Soc. Rev.*, 2022, **51**, 4583–4762.

21 J. C. Cardozo, D. R. da Silva, C. A. Martínez-Huitle, M. A. Quiroz and E. V. Dos Santos, *Materials*, 2022, **15**, 7445.

22 J. E. L. Santos, D. R. da Silva, C. A. Martínez-Huitle, E. V. dos Santosa and M. A. Quiroz, *RSC Adv.*, 2020, **10**, 37947–37955.

23 Y. Kim, E. W. Lees and C. P. Berlinguette, *ACS Energy Lett.*, 2022, **7**, 2382–2387.

24 Z. Zhang, L. Melo, R. P. Jansonius, F. Habibzadeh, E. R. Grant and C. P. Berlinguette, *ACS Energy Lett.*, 2020, **5**, 3101–3107.

25 M. D. Merrill and Ralph C. Dougherty, *J. Phys. Chem. C*, 2008, **112**, 3655–3666.

26 C. C. L. McCrory, S. Jung, J. C. Peters and T. F. Jaramillo, *J. Am. Chem. Soc.*, 2013, **135**, 16977–16987.

27 C. C. L. McCrory, S. Jung, I. M. Ferrer, S. M. Chatman, J. C. Peters and T. F. Jaramillo, *J. Am. Chem. Soc.*, 2015, **137**, 4347–4357.

28 J. Du, A. Fiorani, T. Inagaki, A. Otake, M. Murata, M. Hatanaka and Y. Einaga, *JACS Au*, 2022, **2**, 1375–1382.

29 J. Du, A. Fiorani and Y. Einaga, *Sustainable Energy Fuels*, 2021, **5**, 2590–2594.

30 Y. Einaga, *Electrochemistry*, 2022, **90**, 101002.

31 N. Ikemiya, K. Natsui, K. Nakata and Y. Einaga, *ACS Sustainable Chem. Eng.*, 2018, **6**, 8108–8112.

32 K. Natsui, H. Iwakawa, N. Ikemiya, K. Nakata and Y. Einaga, *Angew. Chem., Int. Ed.*, 2018, **57**, 2639–2643.

33 C. C. L. McCrory, S. Jung, I. M. Ferrer, S. M. Chatman, J. C. Peters and T. F. Jaramillo, *J. Am. Chem. Soc.*, 2015, **137**, 4347–4357.

34 S. U. M. Khan, M. Al-Shahry and W. B. Ingler Jr., *Science*, 2002, **297**, 2243–2245.

35 J. H. Park, S. Kim and A. J. Bard, *Nano Lett.*, 2006, **6**, 24–28.

36 A. Ghicov, H. Tsuchiya, J. M. Macak and P. Schmuki, *Electrochem. Commun.*, 2005, **7**, 505–509.

37 B. Parkinson, *Acc. Chem. Res.*, 1984, **17**, 431–437.

38 R. H. Coridan, A. C. Nielander, S. A. Francis, M. T. McDowell, V. Dix, S. M. Chatman and N. S. Lewis, *Energy Environ. Sci.*, 2015, **8**, 2886–2901.

39 L. Salmon, S. Iran Rocha, F. Elisabete, V. Mikhail, C. Joaquim and T. Carlos José, *Solid State Commun.*, 2022, **341**, 114573.

40 T. D. Burleigh, *Corrosion*, 1989, **45**, 464–472.

41 E. Barborini, A. M. Conti, I. Kholmanov, P. Piseri, A. Podestà, P. Milani, C. Cepek, O. Sakho, R. Macovez and M. Sancrotti, *Adv. Mater.*, 2005, **17**, 1842–1846.

42 Z. Zhao, R. V. Goncalves, S. K. Barman, E. J. Willard, E. Byle, R. Perry, Z. Wu, M. N. Huda, A. J. Moulé and F. E. Osterloh, *Energy Environ. Sci.*, 2019, **12**, 1385–1395.

43 Y. V. Pleskov, V. M. Mazin, Y. E. Evstefeeva, V. P. Varnin, I. G. Teremetskaya and V. A. Laptev, *Electrochem. Solid-State Lett.*, 2000, **3**, 141–143.

44 R. Beranek, *Adv. Phys. Chem.*, 2011, 786759.

45 A. Hankin, F. E. Bedoya-Lora, J. C. Alexander, A. Regoutz and G. H. Kelsall, *J. Mater. Chem. A*, 2019, **7**, 26162–26176.

46 Y. Xu and M. A. A. Schoonen, *Am. Mineral.*, 2000, **85**, 543–556.

47 M. A. Butler and D. S. Ginley, *J. Electrochem. Soc.*, 1978, **125**, 228–232.

48 J. M. Bolts and M. S. Wrighton, *J. Phys. Chem.*, 1976, **80**, 2641–2645.

49 Gurudayal, J. Bullock, D. F. Srankó, C. M. Towle, Y. Lum, M. Hettick, M. C. Scott, A. Javey and J. Ager, *Energy Environ. Sci.*, 2017, **10**, 2222–2230.

50 X. Zhou, R. Liu, K. Sun, Y. Chen, E. Verlage, S. A. Francis, N. S. Lewis and C. Xiang, *ACS Energy Lett.*, 2016, **1**, 764–770.

51 S. Y. Chae, S. Y. Lee, S. G. Han, H. Kim, J. Ko, S. Park, O.-S. Joo, D. Kim, Y. Kang, U. Lee, Y. J. Hwang and B. K. Min, *Sustainable Energy Fuels*, 2020, **4**, 199–212.